Non-invasive analysis of motor neurons controlling the intrinsic and extrinsic muscles of the hand

PAPER

Non-invasive analysis of motor neurons controlling the intrinsic and extrinsic muscles of the hand

IOP Publishing J. Neural Eng. 17 (2020) 046033 https://doi.org/10.1088/1741-2552/aba6db

Journal of Neural Engineering

OPEN ACCESS

RECEIVED
25 February 2020

REVISED
7 July 2020

ACCEPTED FOR PUBLICATION
16 July 2020

PUBLISHED
11 August 2020

PAPER

Non-invasive analysis of motor neurons controlling the intrinsic and extrinsic muscles of the hand

Simone Tanzarella[1], **Silvia Muceli**[2], **Alessandro Del Vecchio**[1], **Andrea Casolo**[1] **and Dario Farina**[1]

[1] Department of Bioengineering, Imperial College London, London, United Kingdom
[2] Division of Signal Processing and Biomedical Engineering, Department of Electrical Engineering, Chalmers University of Technology, Gothenburg, Sweden

E-mail: d.farina@imperial.ac.uk

Keywords: HD-sEMG, hand muscles, neural drive, motor units, neural interface

Abstract

Objective. We present a non-invasive framework for investigating efferent commands to 14 extrinsic and intrinsic hand muscles. We extend previous studies (limited to a few muscles) on common synaptic input among pools of motor neurons in a large number of muscles. *Approach*. Seven subjects performed sinusoidal isometric contractions to complete seven types of grasps, with each finger and with three combinations of fingers in opposition with the thumb. High-density surface EMG (HD-sEMG) signals (384 channels in total) recorded from the 14 muscles were decomposed into the constituent motor unit action potentials. This provided a non-invasive framework for the investigation of motor neuron discharge patterns, muscle coordination and efferent commands of the hand muscles during grasping. Moreover, during grasping tasks, it was possible to identify common neural information among pools of motor neurons innervating the investigated muscles. For this purpose, principal component analysis (PCA) was applied to the smoothed discharge rates of the decoded motor units. *Main results*. We found that the first principal component (PC1) of the ensemble of decoded motor neuron spike trains explained a variance of (53.0 $\pm$ 10.9) % and was positively correlated with force (R = 0.67 $\pm$ 0.10 across all subjects and tasks). By grouping the pools of motor neurons from extrinsic or intrinsic muscles, the PC1 explained a proportion of variance of (57.1 $\pm$ 11.3) % and (56.9 $\pm$ 11.8) %, respectively, and was correlated with force with R = 0.63 $\pm$ 0.13 and 0.63 $\pm$ 0.13, respectively. *Significance.* These observations demonstrate a low dimensional control of motor neurons across multiple muscles that can be exploited for extracting control signals in neural interfacing. The proposed framework was designed for hand rehabilitation perspectives, such as post-stroke rehabilitation and hand-exoskeleton control.

1. Introduction

The human hand is a neuromuscular-skeletal system fundamental for interacting with the external environment and for communicating. Its complexity has been investigated functionally and biomechanically (Napier 1956, Landsmeer 1962, Iberall 1987, Della Santina *et al* 2017) as well as in neuromechanical modelling studies (Santello *et al* 2013, Valero-Cuevas and Santello 2017). Hand functions can be compromised by sensory-motor impairment, e.g. resulting from stroke (Meyer *et al* 2014). In case of impairment, given the hand complexity, specific rehabilitation systems (e.g. based on robotics) may be necessary in addition to conventional therapy (Kwakkel 2008).

The hand is controlled by numerous extrinsic and intrinsic muscles. Due to this complexity, few studies have investigated the activation of both extrinsic and intrinsic muscles responsible for hand movements (Huesler and Maier 2000, Weiss and Flanders 2004, Ajboye and Weir 2009). Aijboye and Weir(2009) combined surface and intramuscular electromyography (EMG) to detect the global activation level of intrinsic and extrinsic muscles. However, surface EMG amplitude provides an approximate indication of the actual muscle activation and more importantly it is only crudely associated to the underlying motor unit activities (Farina *et al* 2004). A more accurate estimation of the efferent command (neural drive) received by the muscle is obtained investigating the

recruitment and firing patterns of motor units, which constitute the final pathway of the nervous system. This analysis has been applied to single hand muscles, such as the first dorsal interosseous (FDI) (Enoka and Fuglevand 2001) and abductor digiti minimi (ADM) (Negro *et al* 2009), typically using intramuscular electromyography. The studies by Weiss (2004) and Huesler (2000) are the only reports that attempted to estimate single motor unit activity from multiple intrinsic and extrinsic muscles, with surface and intramuscular EMG, respectively. However, these studies were successful in few subjects (four and five respectively) and muscles (respectively 7 and 14, but in the latter case these were only muscles actuating the thumb and the index finger).

A non-invasive way to assess neural strategies and motor unit control is provided by high-density surface EMG (HD-sEMG) (Farina *et al* 2004, 2014a). HD-sEMG is recorded with grids of closely spaced electrodes over the skin (Merletti and Muceli 2019) and it allows segmentation of surface EMG 2D maps and decomposition into the constituent motor unit action potential trains (Merletti *et al* 2010, Stegeman 2012). HD-sEMG decomposition enables the decoding of the neural drive to muscles (Negro *et al* 2009, Farina *et al* 2010) and the estimation of common drive (Nordstrom *et al* 1992, De Luca and Erim 1994, Negro *et al* 2009, Farina and Negro 2015). HD-sEMG was used to study the global muscle activity of the hand, without decomposition, for single finger classification (Celadon *et al* 2015) and in proportional single finger control (Celadon *et al* 2016). It was also applied to extract the neural drive to forearm muscles actuating the wrist (Kapelner *et al* 2017) and fingers (Del Vecchio *et al* 2019).

Here, we propose for the first time a non-invasive framework for the investigation of motor neuron discharge patterns, muscle coordination and efferent commands to extrinsic and intrinsic hand muscles for a total of 14 muscle compartments. By applying this framework to seven grasp types, we demonstrate that it enables to discriminate the location of the electrical activity of single motor units among the investigated muscles and to determine common neural information among pools of motor units of the main intrinsic and extrinsic muscles actuating the hand. The framework is proposed for future applications in hand rehabilitation, such as post-stroke rehabilitation and hand-exoskeleton control. The electrode configuration chosen for this study can indeed lead to a wearable device to be integrated with other rehabilitation technologies.

2. Methods

2.1. Subjects

Seven healthy men (age, 27.0 ± 2.2 yrs; weight, 79.0 ± 8.3 kg; height, 180.1 ± 5.0 cm) volunteered to the experiment after signing an informed consent. The study protocol and procedures were approved by the Imperial College London Research Ethics Committee (approval no. 18IC4685) and conformed to the requirements of the *Declaration of Helsinki*.

2.2. HD-sEMG

EMG signals were recorded from extrinsic and intrinsic hand muscles with six grids of 64 surface EMG electrodes each, with electrodes arranged in a 13 × 5 configuration and one electrode missing at the corner (OT Bioelettronica, Torino, Italy), for a total of 384 electrodes, as depicted in figure 1(a). Two 13 × 5 grids with 8-mm inter-electrode distance (IED) were placed over the extrinsic muscles (extensor digitorum communis and flexor digitorum superficialis). Four grids with 13 × 5 electrodes at 4-mm IED were placed over the following intrinsic muscles: FDI, the other three dorsal interossei, the thenar and the ADM.

Prior to electrode positioning, the subject was asked to repeatedly move the fingers in order to identify the muscle belly locations through palpation. To identify the extensor and flexor digitorum, the subject was asked to move the little and the index finger, to assure the covering of all four compartments of these muscles. Before placing the electrodes, the skin over the forearm and the hand was shaved and cleansed with alcohol with 70% ethanol to minimize electrode-skin impedance. Grids were attached to the skin with disposable bi-adhesive foam layers filled with conductive paste and were secured with tape. An overview of the positioning of the grids on the tested muscles is shown in figure 1(a).

The grids targeting the extensor (EXT) and flexor (FLX) digitorum muscles were placed on the dorsal and ventral sides of the forearm, respectively, with the shortest side aligned to the ulna bone. The first grid was placed in the most proximal third of the forearm and the second grid distal to the first. Due to its length (about 10 cm), the grid on the dorsal side extended over the extensor carpi radialis and extensor carpi ulnaris longus muscles, while the grid on the ventral side extended over the flexor carpi radialis and flexor carpi ulnaris. The grid over the thenar muscles (THE) had its shortest side along the thumb metacarpal bone and extended on the palmar side of the hand to cover the opponens pollicis, flexor pollicis brevis, and abductor pollicis brevis muscles. The FDI was covered with a grid aligned with its longer side on the dorsal side of the thumb metacarpal bone and the ADM with a grid along the muscle fibers. Finally, the grid over the II, III and IV dorsal interossei (DI) was mounted in the middle between the index metacarpal bone and the little metacarpal bone, equidistant from the wrist and the knuckles. Thus, a total of 14 muscles, three for each grid on the forearm, the three composing the thenar, the four interossei and ADM, were recorded. The acronyms for each grid electrodes

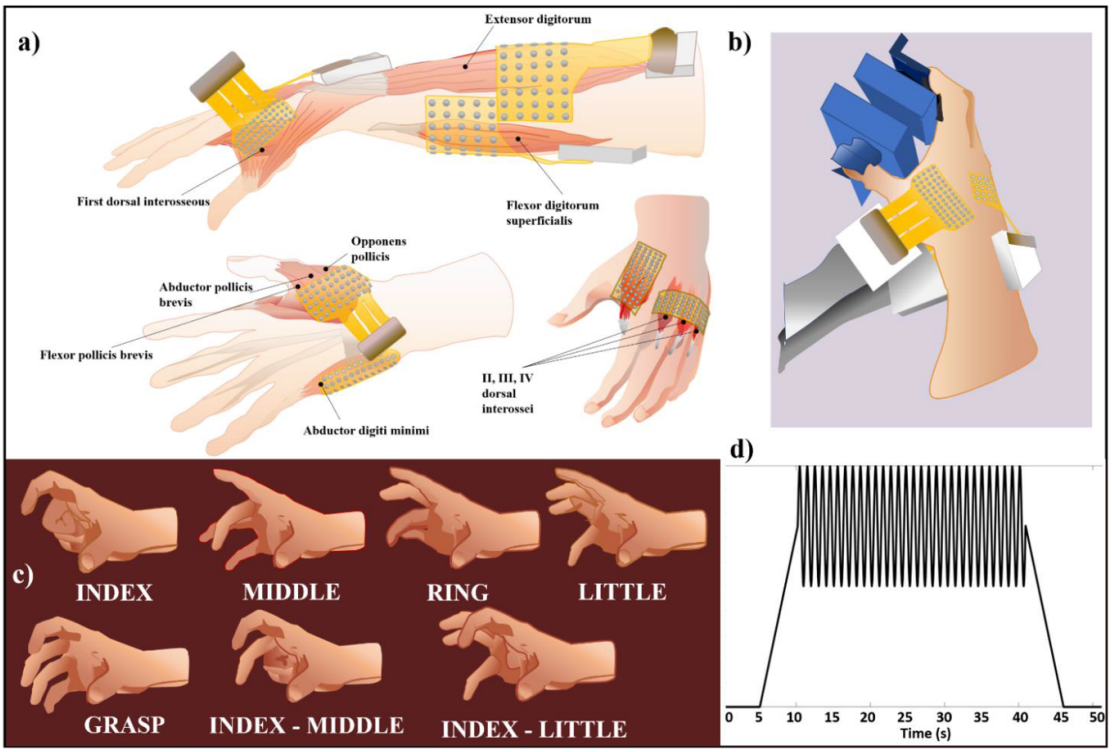

Figure 1. Experimental setup and protocol. (a) The layout of the electrode grids over the first dorsal interosseus, II–IV interossei, abductor digiti minimi, thenar, extensor digitorum communis, and flexor digitorum superficialis muscles. (b) The experimental setup depicting the custom hand-dynamometer. (c) The different types of combinations of fingers in opposition with the thumb in the tested grasps. (d) Example of the sinusoidal force cue followed by the subjects. The cue started after 2 min of rest.

and the corresponding recorded muscles are reported in table 1.

The electrode grids were connected to a multi-channel EMG amplifier (Quattrocento, OT Bioelettronica, Torino, Italy) through 64-channel impedance-adapters with a gain of 5 V/V. EMG signals were recorded in monopolar derivation, amplified with a gain of 150, band-pass filtered between 10 and 900 Hz, sampled at 2048 Hz and A/D converted on 16 bits. A single reference electrode was placed on the wrist of the tested arm.

The forces exerted by the fingers were measured by two load sensors (ATI Industrial Automation, Apex, NC) and recorded through a 12-bit A/D converter board (sampling frequency 2048 Hz, PCI-6225, National Instruments, Austin, TX). Load cells were fixed coaxially in a custom-made hand support by means of two plastic handles for positioning the thumb and a combination of the other fingers (figure 1(b)), according to the tasks represented in figure 1(c).

2.3. Experimental protocol

Subjects sat in a comfortable posture with the forearm and the hand restrained in a brace so that the wrist was kept in a neutral position and all the involved muscles were relaxed during the rest condition. The custom hand-dynamometer (figure 1(b)) was fixed stably on the experimental table. A screen in front of the subject was used to visualize the target force and to provide feedback on the exerted force. The protocol consisted in performing seven types of grasps simultaneously activating the thumb, with one or more fingers opposed to the thumb (figure 1(c)) to press against the two load cells. The subject performed four tasks with the thumb and each other finger. Moreover, they performed three additional grasps, with all fingers, with the thumb and index and middle finger, and with the thumb and index and little finger. The three combined grasps corresponded respectively to the palmar and tripod pinch which are commonly used in daily life activities as well as an unusual grasp.

Subjects were asked to produce the maximal force twice for each finger combination, with a rest of 1 min between attempts. The highest recorded force was considered as the maximal voluntary contraction (MVC). Then, subjects were instructed to match sinusoidal force trajectories, opposing the thumb and the other combination of fingers. For each combination of fingers, the subject had to follow a 30 s-long sinusoidal force profile in the peak-to-peak range 10%–20% MVC (figure 1(d)), with a frequency of 1 Hz and followed by a rest of 2 min. The task was preceded and followed by a 5-s ramp contraction to reach the target level (15% MVC) and return to the rest position (null force), respectively. The sequence of tasks was randomized. All the contractions, both

for the MVC recording and for all the trials, were isometric.

2.4. Signal processing

EMG signals were digitally filtered between 20 and 500 Hz with a 4th-order Butterworth filter and then the convolution kernel compensation (CKC) algorithm (Holobar and Zazula 2007) was used to decompose the signals into the constituent trains of motor unit action potentials. Decomposition was applied separately to the data recorded in each trial and separately to the 64 channels of each grid. Only the central 30 s of the tasks were considered for the analysis. The results of the decomposition were manually inspected and validated by experienced investigators, by discarding all the motor units with pulse-to-noise ratio (PNR) (Holobar *et al* 2014) lower or equal than 25 dB (i.e. with accuracy in the confidence interval of 0–70%) or with less than 60 peaks (i.e. with mean discharge rate of 2 Hz), by removing the false-positive peaks over the physiological threshold of firing (35–40 Hz) and by checking evident false-negative undetected peaks, by analyzing each motor unit innervation pulse train (IPT) (Holobar and Zazula 2007). For each recording, the mean firing rate (MFR) was computed as the mean of the reciprocal of the inter-spike interval (ISI) (Nordstrom *et al* 1992) for each pair of consecutive spikes. The MFR was also computed by grouping, for each motor unit, the spikes during increasing and decreasing force. The force phases were segmented by a zero-crossing threshold on the derivative of the low-pass filtered force signal.

Each spike train was represented as a binary signal, with 1 representing the occurrence of a discharge and 0 otherwise. To have a continuous representation of the neural activity and, thus, an estimation of the instantaneous FR, the spike trains were smoothed by convolving the binary spike trains with a 400-ms Hanning window (De Luca 1985, Negro *et al* 2009). The smoothed cumulative spike train was obtained by summing sample by sample the smoothed spike trains across motor units. The delay between the force signal and the smoothed cumulative spike trains was also computed for each trial as the time lag corresponding to the peak of the cross-correlation function.

To locate each motor unit under the relative electrode grid from which it was detected, we averaged the epochs of signal, for each channel of the grid, segmented around each firing of the considered motor unit with a 103-samples-wide window (50 ms), as described in Farina *et al* 2002.

2.5. Common drive quantification by PCA

The common input to pools of motor neurons innervating different muscles was investigated by principal component analysis (PCA) (Negro *et al* 2009, Farina and Negro 2015). First, all motor units extracted separately from the grids were pooled together. We also analysed separately the pool of the intrinsic muscles and of the extrinsic muscles. Then, PCA was applied to the smoothed spike trains to extract common components in the behaviour of the motor units. For this purpose, the smoothed discharge rates were factorized by a singular value decomposition PCA.

Singular value decomposition (SVD) is a matrix factorization technique and can be used to compute PCA alternatively than performing an eigenvalue decomposition of the covariance matrix (Negro *et al* 2009), to obtain a more accurate result and a more efficient computation of the PCA (Jolliffe and Cadima 2016). SVD applied to a real-valued matrix $X \in R^{n\times m}$ provides the following factorization (Brunton and Kutz 2019):

$$X = U\Sigma V^T,$$

where $U \in R^{n\times n}$ and $V \in R^{m\times m}$ are unitary matrices with orthonormal columns, $\Sigma \in R^{n\times m}$ is a matrix with real, nonnegative entries on the diagonal and zeros everywhere else, and V^T is the transpose of V. The dimensions n and m are respectively for the observation and for the variables, thus, in our case, they are respectively indexes for the number of samples in the 30-s intervals of analysis and the number of motor units. The scores (here, the time-varying components shown in figure 2(b)) are the columns of the matrix product $U\Sigma$, and the coefficient (here, the weights representing the contribution of each motor unit for each component) are the columns of V. U is the standardized version of the PC scores, and the percentage of each single value in Σ over the trace of Σ provides the explained variance of each component (after sorting Σ in descendent order) (Jolliffe and Cadima 2016). PCA was computed among all the motor units, separately for each recording.

3. Results

table 2 reports the descriptive statistics on the number of identified motor units and MFR across the seven subjects for the seven tasks. The number of motor units identified per grid was 6.4 ± 3.4, MFR was 14.4 ± 8.8 Hz, and PNR was 30.4 ± 4.8 dB. Values for MFR were all in the physiological range and the number of identified motor units changed for different tasks. In general, the number of motor units which were detected from extrinsic muscles was smaller than from intrinsic muscles. The table also distinguishes the MFR computed during increasing and decreasing phases of the force signal (represented in figure 2), to provide a further information about discharge of motor units for each grid during different tasks. Globally, MFR was 15.9 ± 9.7 Hz during increasing force and 13.2 ± 8.6 Hz during decreasing force. Mean values reported in table 2 are in general greater for increasing force than for decreasing force for the grids FDI, DI, ADM and EXT for all the tasks (except

Table 1. Acronyms for each electrode grid and corresponding muscles from which each grid recorded EMG.

Grid acronym	Recorded muscles
FDI	First dorsal interosseous
DI	II, III, IV dorsal interossei
ADM	Abductor digiti minimi
THE	Thenar muscles: opponens (OPP), flexor pollicis brevis (FPB), abductor pollicis brevis (APB)
EXT	Extensor carpi ulnaris, extensor digitorum communis, extensor carpi radialis
FLX	Flexor carpi ulnaris, flexor digitorum superficialis, flexor carpi radialis

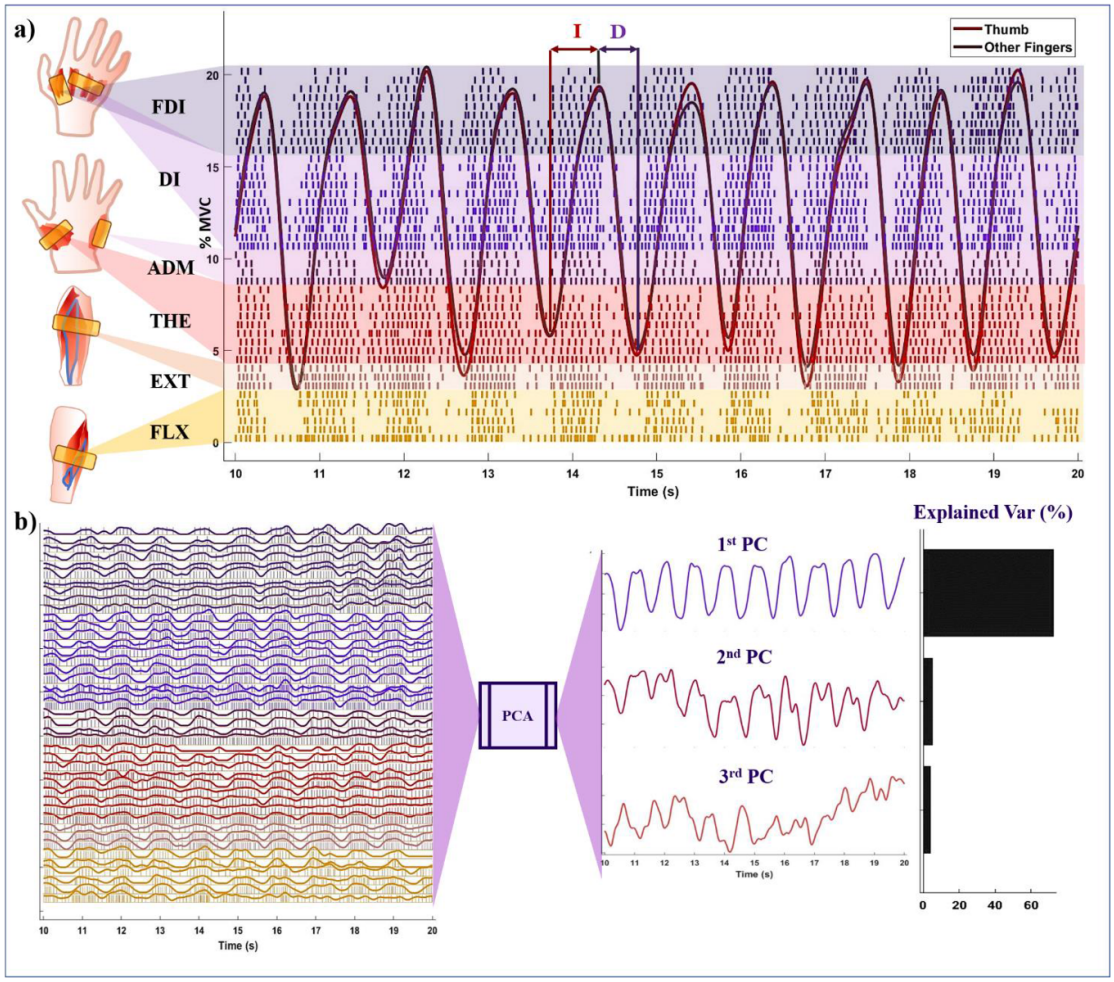

Figure 2. (a) Example of motor unit spike trains extracted from the investigated muscles for one representative subject performing a grasp with a sinusoidal isometric contraction. The exerted force measured by the two load cells is represented as % MVC. One example of increasing (I) and decreasing (D) interval of force is represented for one cycle of sinusoidal force. (b) The same spike train pool is smoothed and PCA is applied. The first three principal components are represented and the respective values of explained variance are reported. See table 1 for the muscle definition.

for ADM in middle-thumb grip). For the grids THE and FLX more variability can be observed.

Figure 2(a) shows a set of motor unit spike trains from all the investigated muscles for a representative subject during a five-digit grasp task. The force signal, respectively for the thumb and the other four fingers, is represented as % MVC. figure 2(b) shows the smoothed continuous signals from the spike trains as well as the result of PCA. In this representative example, the first principal component (PC1) explained approximately 70% of the total variance, whereas the second and third components explained less than 5% of the variance. Therefore, the activity of all the decoded motor neurons during this task could be reduced to one principal component signal. Moreover, in this example, the delays between the smoothed cumulative spike trains and the generated force for the six grids were 235 ms (grid on FDI), 225 ms (dorsal interossei), 225 ms (ADM), 201 ms (thenar), 219 ms (extensor muscles), and 236 ms (flexor muscles), which correspond to previous neuromuscular latencies estimated from motor unit and force recordings in the FDI (Erimaki *et al* 2013, Del Vecchio *et al* 2018).

Figure 3 shows the localization of muscle units under the grid area, obtained by triggering the averaging of the motor unit action potentials with the time occurrences of the motor unit discharges for each EMG channel (Farina *et al* 2002). Examples are presented for the II, III and IV dorsal interossei (DI), under the same grid, and for the opponens pollicis (OPP), abductor pollicis brevis (APB) and the flexor pollicis brevis (FPB), the three parts of the thenar. One example is also presented for the group of the extensor muscles (EXT), by showing the position of the different muscles in the forearm. Finally, one example is shown for FDI and ADM, which are the only muscles under their respective grid, but have motor units which can be in different locations depending on the innervation zone. For ADM, the spike-triggered average (STA) is also useful to assess the propagation of the motor unit action potentials along the fibres (Merletti *et al* 2010), as can be seen in the figure. The action potential time window for the STA is the same for all grids (50 ms).

Figure 4 shows the strength of the PC1 for all motor units extracted from all muscles and its association with the force exerted by the fingers. The PCA was performed separately for each recording, as explained in the Methods, and then the results were averaged across recordings. figure 4(a) shows the comparison between PC1 and the force signals. Each trace is normalized by its maximum value, to emphasize the time course of the signals rather than their amplitude. figure 4(b) shows the mean and standard deviation of the variance explained by the first 10 principal components extracted by PCA from the neural drive in 49 recordings, for all subjects. PC1 is much higher with respect to the other components, with an explained variance of (53.0 ± 10.9) % for all the motor units pooled together, (57.1 ± 11.3) % by pooling the extrinsic motor units and (56.9 ± 11.8) % by pooling the intrinsic motor units. The second component explained only (11.5 ± 4.5) % of the variance for the motor units pooled together. figure 4(c) shows the spectral coherence between the PC1 and the finger combination force (in opposition with the thumb) separately for each task across subjects. Thus, each averaged spectral coherence is calculated over 7 recordings. The peak at 1 Hz corresponds to the frequency of the sinusoidal contractions performed by the subjects.

Table 3 reports the mean and standard deviation across all subjects of the cross-correlation peak between finger combination force (in opposition with the thumb) and PC1, both separately for each task and across all tasks. The values in table 3 are computed over the interval of 30 s. Eliminating the first and last 10 s of the sinusoidal contraction and maintaining the central 10 s of recording only, i.e. the most stable portion of the task, the cross-correlation values further increased compared to the total 30 s and reached the values of 0.70 ± 0.14 (All), 0.68 ± 0.16 (Extr), 0.68 ± 0.16 (Intr), 0.67 ± 0.17 (FDI), 0.65 ± 0.17 (DI), 0.58 ± 0.23 (ADM), 0.54 ± 0.19 (THE), 0.69 ± 0.17 (EXT), and 0.61 ± 0.18 (FLX).

Cross-correlation peak values for FDI in all the tasks involving the index finger, i.e. five-digits grasp, index-thumb pinch, index-little-thumb grip and index-middle-thumb grip, were respectively 0.62 ± 0.09, 0.67 ± 0.13, 0.67 ± 0.05, 0.64 ± 0.12. Values for ADM in all the tasks involving the little finger, i.e. five-digits grasp, index-little-thumb grip and little-thumb pinch were, respectively, 0.48 ± 0.16, 0.51 ± 0.09, 0.62 ± 0.12, all exceeding the average value computed across all tasks.

The PCA loads, representing the contribution of motor units to PC1, are shown for all the subjects in figure 5. As explained in Methods, PC1 is extracted for each EMG recording across a unique pool of motor units from all muscles. They are represented in boxplots after being normalized by the maximum, grouped by grid and sorted before averaging. The number of loads reflect the number of motor units per grid and per task, therefore this information corresponds to table 3. However, figure 5 provides also the information about how much each motor unit is represented in PC1, with some units contributing with a negative weight. Across all subjects, 78% of the motor units contributed to PC1 with a positive load. The muscles from where the greatest number of motor units contributed with negative loads were under the grids FLX and DI, with respectively 26% and 21% of the total motor units.

4. Discussion

This study presents a framework to investigate how motor units are recruited in the main muscles actuating the hand, both intrinsic and extrinsic. The novelty introduced by this framework is the quantification of the common neural drive from more than ten muscles concurrently (the four dorsal interossei, abductor digiti minimi, the three muscles composing the thenar, extensor digitorum communis, flexor digitorum superficialis, plus other muscles actuating the wrist which are recorded by the grids over the forearm) in a non-invasive way. In particular, results about motor unit discharge patterns of the four dorsal interossei from HD-sEMG are presented for the first time. With this framework we confirm and expand the results of previous studies investigating common synaptic input among pool of motor units of only one or few muscles (Nordstrom *et al* 1992, De Luca and Erim 1994, Negro *et al* 2009), or with many muscles but a single motor unit observed at a time (Weiss and Flanders 2004, Husler *et al* 2000). We assessed common synaptic input among motor neurons innervating 14 muscles. We choose to examine the muscles of the hand because of the vast number of applications in rehabilitation and

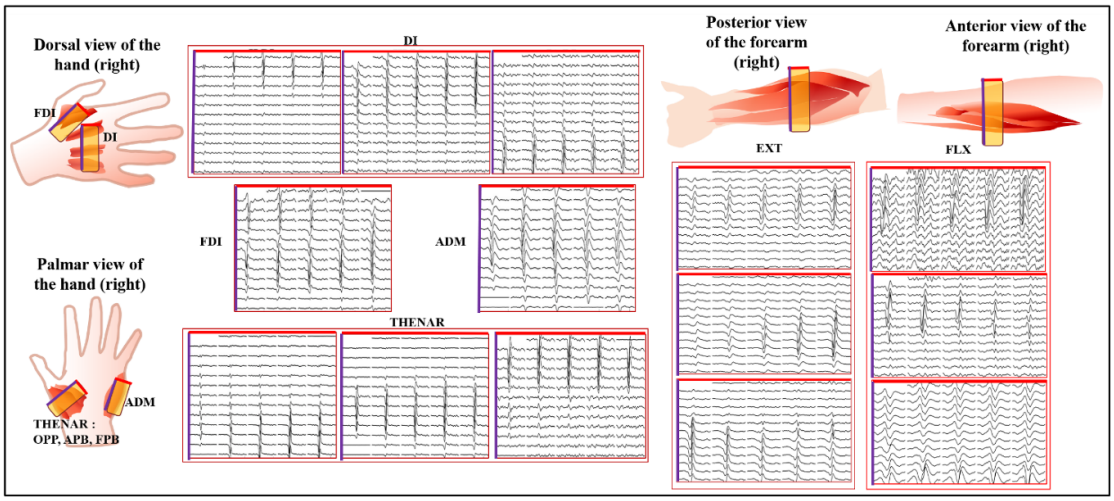

Figure 3. Examples of spike-triggered average for motor units of one representative subject for different electrode grids. The action potential waveforms as detected by the surface grids are shown for individual motor units of the dorsal interossei (II, III and IV DI), thenar, composed by flexor pollicis brevis (FPB), abductor pollicis brevis (APB), and opponens pollicis (OPP), first dorsal interosseus (FDI), abductor digiti minimi (ADM) and the extensor (EXT) and flexor (FLX) muscles groups. See table 1 for the muscle definition.

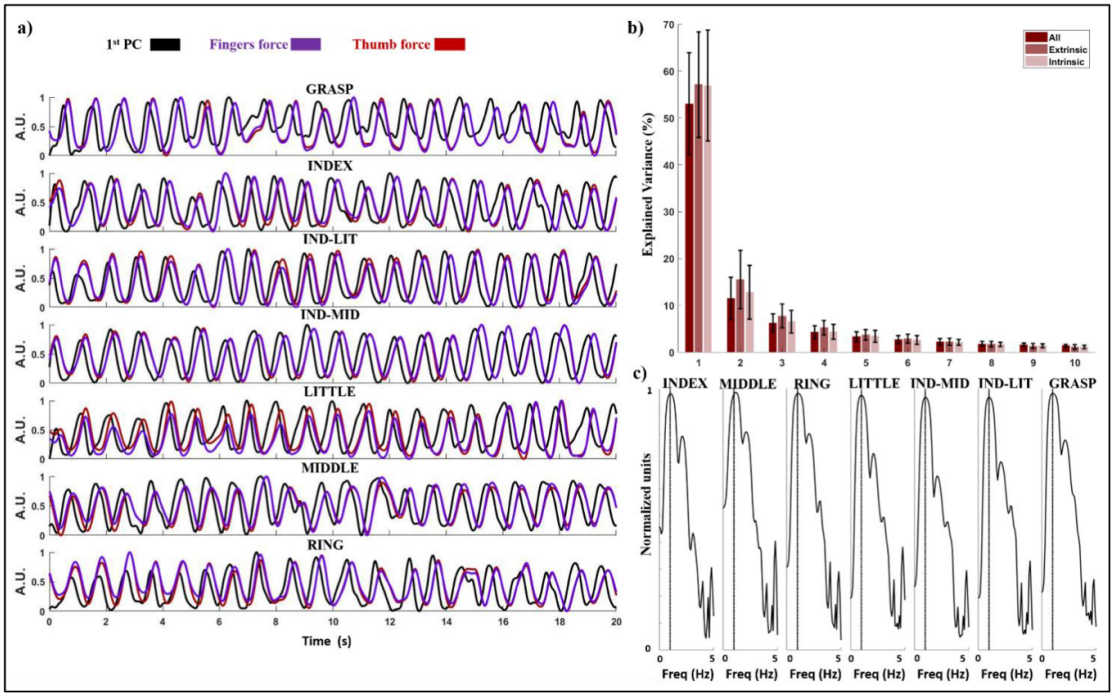

Figure 4. Analysis of the common drive among motor units from different extrinsic and intrinsic muscles of the hand, extracted by using PCA. In (a), for one subject, the first principal component (PC1) is compared with the force measured for the thumb and the other combinations of fingers. In (b), for all seven subjects, the mean and standard deviation of the percentage of explained variance for the first ten principal components is represented. In (c), for all seven subjects, the averaged spectral coherence between the PC1 and the force developed for each type of task is represented between 0 and 5 Hz. See figure 1(c) for the task definition. A.U.: arbitrary unit.

considering the complexity inherent in this part of the body presenting many degrees of freedom. Common amount of neural information among the motor neurons of all the muscles was quantified by PCA computed from the motor unit smoothed discharge patterns. PCA was computed intra-task and the results were averaged across trials and subjects, to assess the average common neural drive when performing grasps and pinches with different combinations of fingers. The results showed the possibility of estimating descending commands to multiple spinal levels to assess global synergistic control of motor neurons.

The use of the proposed framework indicated a low dimensionality in control of the motor neuron pools of the multiple muscles investigated during

Table 3. Mean and standard deviation of the cross-correlation peaks between force and PC1 over 30 s for each task. Results are for all subjects for PC1 calculated by pooling all the motor units and by pooling motor units within each single electrode grid. See table 1 for the muscle definition and figure 1(c) for the task definition. Extr: extrinsic muscles; Intr: intrinsic muscles.

	GRASP	INDEX	IND-LIT	IND-MID	LITTLE	MIDDLE	RING	ALL TASK
All	0.62 ± 0.13	0.71 ± 0.11	0.62 ± 0.14	0.67 ± 0.10	0.69 ± 0.05	0.69 ± 0.10	0.67 ± 0.08	0.67 ± 0.10
Extr	0.60 ± 0.13	0.61 ± 0.15	0.64 ± 0.10	0.63 ± 0.13	0.66 ± 0.15	0.65 ± 0.13	0.59 ± 0.14	0.63 ± 0.13
Intr	0.61 ± 0.14	0.69 ± 0.11	0.61 ± 0.14	0.66 ± 0.10	0.61 ± 0.10	0.68 ± 0.10	0.57 ± 0.19	0.63 ± 0.13
FDI	0.62 ± 0.09	0.67 ± 0.13	0.67 ± 0.05	0.64 ± 0.12	0.57 ± 0.12	0.64 ± 0.11	0.49 ± 0.15	0.61 ± 0.12
DI	0.60 ± 0.09	0.65 ± 0.13	0.59 ± 0.07	0.64 ± 0.10	0.47 ± 0.16	0.68 ± 0.09	0.52 ± 0.19	0.59 ± 0.14
ADM	0.48 ± 0.16	0.28 ± 0.12	0.51 ± 0.09	0.44 ± 0.13	0.62 ± 0.12	0.39 ± 0.13	0.46 ± 0.20	0.46 ± 0.16
THE	0.48 ± 0.10	0.44 ± 0.22	0.49 ± 0.13	0.52 ± 0.12	0.41 ± 0.16	0.54 ± 0.13	0.44 ± 0.16	0.47 ± 0.15
EXT	0.57 ± 0.11	0.61 ± 0.13	0.63 ± 0.08	0.63 ± 0.12	0.61 ± 0.15	0.60 ± 0.20	0.59 ± 0.08	0.61 ± 0.12
FLX	0.58 ± 0.12	0.52 ± 0.12	0.56 ± 0.13	0.53 ± 0.10	0.59 ± 0.21	0.57 ± 0.08	0.53 ± 0.15	0.56 ± 0.13

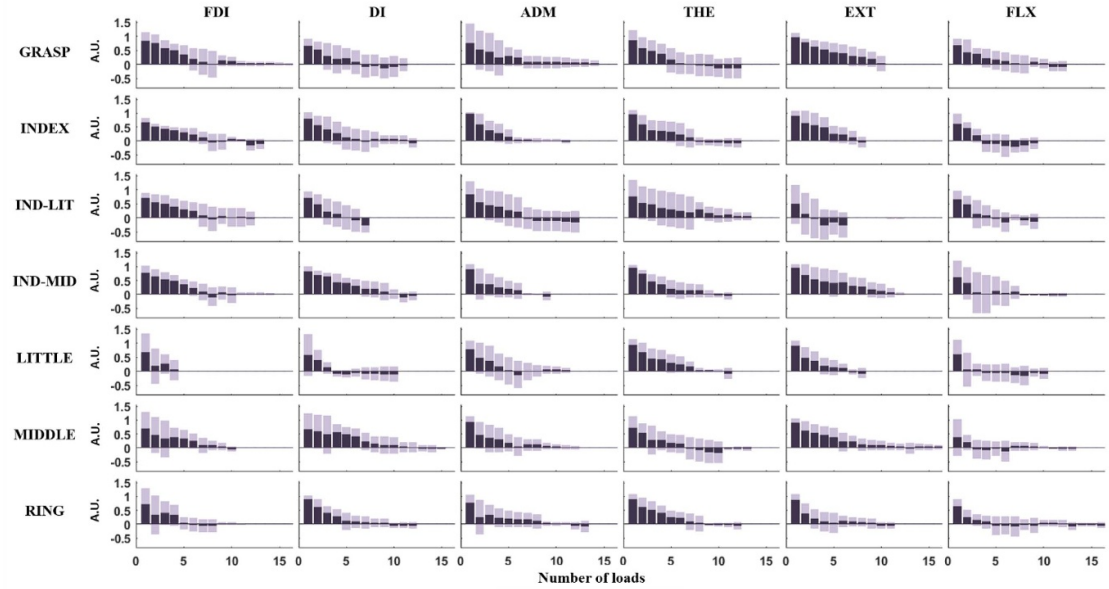

Figure 5. Mean (dark bars) and standard deviation (light bars) of the sorted PCA loads grouped for each grid for PC1 across the subjects. These loads represent how each motor unit contributes to PC1 and may have a negative value representing a contribution in counterphase with respect to the other motor units of the pool. For each row, representing a task, the averaged loads are extracted by PCA from the same EMG recording, then normalized by the maximum, grouped by grid (columns) and descently sorted in each boxplot. See table 1 for the muscle definition and figure 1(c) for the task definition.

grasping. The variance explained by the first principal component PC1 of the complete set of motor neuron spike trains across the different grasp types was indeed very high ((53.0 ± 10.9)%) (figure 4(b)). Moreover, PC1 was highly correlated with force (table 3). The value of explained variance for PC1 was higher than the value previously reported by Negro *et al* (2009) for a single muscle (ADM) (44.2 ± 7.5)% for the abduction of the little finger. Moreover, also the correlation between PC1 and force that we have observed across all trials (0.67 ± 0.10, table 3) was greater than the value reported by Negro *et al* (2009) for ADM only (0.63 ± 0.10).

PC1 explained a variance, for all the considered hand muscles, five times greater than the second component, while the third component explained only ~6% and the others <5% of the variance. This result indicates that PC1 is a strong common drive signal sent to all muscles by the central nervous system, underlying a highly synergistic control of grasp. We did not further investigate the individuation of synergies associated to particular degrees of freedom or to particular tasks, nor we aimed to assess the robustness of these synergies and the sensory-motor models behind their behaviour. However, this framework could be used in future studies to assess synergies in motor neurons innervating hand muscles. Here we aimed at assessing how common drive explains force modulation, as it can be observed representatively in figure 4(a). In the perspective of man-machine interfacing applications, PC1 would provide a robust motor-neuron based myoelectric control of grasp (Bergmeister *et al* 2017, Farina *et al* 2017).

We further evaluated the common drive to muscles by separating intrinsic and extrinsic motor units. This is of practical relevance in interfacing prostheses since intrinsic muscles may be missing. We

Table 2. Number of motor units (N MUs), and mean firing rate (MFR) for each task (rows) and for each grid (columns). MFR is reported by considering all the spikes for each motor unit, and by grouping them respectively during the increasing and decreasing phase of the force signal.

		FDI	DI	ADM	THE	EXT	FLX
GRASP	**N MUs**	9.9 ± 3.3	8.1 ± 2.9	5.9 ± 4.0	6.0 ± 3.6	7.7 ± 3.4	7.1 ± 3.5
	MFR (Hz)	13.6 ± 2.5	14.5 ± 3.8	13.0 ± 2.9	14.5 ± 3.6	15.2 ± 3.0	14.9 ± 2.3
	MFR increase (Hz)	15.5 ± 2.7	16.2 ± 3.4	14.5 ± 3.1	14.2 ± 3.3	16.9 ± 3.1	16.0 ± 4.3
	MFR decrease (Hz)	9.9 ± 2.8	10.6 ± 3.7	10.6 ± 3.1	14.1 ± 4.7	13.1 ± 3.5	12.6 ± 3.4
INDEX	**N MUs**	10.1 ± 2.5	7.3 ± 3.1	5.2 ± 3.2	5.8 ± 3.7	5.9 ± 2.1	5.4 ± 2.8
	MFR (Hz)	14.1 ± 3.1	14.8 ± 3.0	12.0 ± 2.4	14.9 ± 2.9	16.0 ± 3.2	13.2 ± 2.1
	MFR increase (Hz)	16.1 ± 3.3	16.9 ± 2.8	13.1 ± 2.4	14.5 ± 3.5	17.6 ± 3.7	13.6 ± 3.7
	MFR decrease (Hz)	11.9 ± 4.1	12.9 ± 3.3	11.6 ± 2.8	14.9 ± 4.7	14.1 ± 3.4	13.5 ± 2.4
IND-LIT	**N MUs**	9.9 ± 2.2	6.0 ± 1.8	6.6 ± 3.6	9.6 ± 2.6	5.9 ± 2.9	6.0 ± 3.1
	MFR (Hz)	12.9 ± 2.8	13.1 ± 3.1	13.9 ± 2.6	15.5 ± 3.2	14.7 ± 2.9	13.2 ± 3.2
	MFR increase (Hz)	14.0 ± 3.9	14.4 ± 3.8	14.8 ± 3.1	15.2 ± 3.8	16.2 ± 3.2	13.7 ± 4.3
	MFR decrease (Hz)	11.3 ± 4.1	12.0 ± 2.8	12.7 ± 3.5	15.7 ± 4.1	13 ± 3.8	12.8 ± 3.0
IND-MID	**N MUs**	9.3 ± 2.4	8.4 ± 2.8	4.4 ± 3.2	5.5 ± 3.6	7.9 ± 2.7	5.4 ± 3.3
	MFR (Hz)	13.3 ± 2.4	13.9 ± 2.1	13.4 ± 3.2	14.8 ± 3.4	15.6 ± 2.6	13.7 ± 2.6
	MFR increase (Hz)	15.1 ± 2.5	15.9 ± 2.3	14.3 ± 3.3	14.5 ± 4.3	17.0 ± 3.0	14.5 ± 4.1
	MFR decrease (Hz)	9.1 ± 3.3	10.0 ± 2.5	13.1 ± 4.7	15.1 ± 5.3	12.9 ± 3.1	12.2 ± 3.3
LITTLE	**N MUs**	3.0 ± 1.3	3.9 ± 3.2	6.1 ± 3.1	5.7 ± 3.5	4.7 ± 2.1	5.3 ± 3.3
	MFR (Hz)	10.8 ± 3.6	11.3 ± 2.1	14.2 ± 1.7	16.8 ± 3.8	14.3 ± 2.7	14.0 ± 3.2
	MFR increase (Hz)	12.6 ± 4.7	12.3 ± 3.0	15.2 ± 2.1	17.2 ± 4.4	15.7 ± 3.2	15.1 ± 3.5
	MFR decrease (Hz)	9.4 ± 2.8	11.2 ± 2.4	13.5 ± 2.6	16.9 ± 4.5	13.7 ± 3.8	13.5 ± 4.2
MIDDLE	**N MUs**	6.2 ± 3.6	8.0 ± 3.7	4.7 ± 4.1	7.8 ± 4.2	6.8 ± 3.4	5.0 ± 4.2
	MFR (Hz)	12.8 ± 3.5	13.4 ± 2.1	13.0 ± 2.8	14.2 ± 3.1	14.3 ± 2.5	12.5 ± 1.8
	MFR increase (Hz)	14.1 ± 4.1	14.7 ± 2.4	13.1 ± 3.3	14.1 ± 3.2	15.7 ± 2.6	13.1 ± 2.3
	MFR decrease (Hz)	11.5 ± 5.0	12.5 ± 3.1	13.5 ± 2.7	14.2 ± 4.3	13.2 ± 3.2	11.5 ± 3.0
RING	**N MUs**	4.7 ± 3.6	5.6 ± 3.5	4.8 ± 4.7	6.7 ± 3.5	5.8 ± 3.9	7.2 ± 4.0
	MFR (Hz)	11.4 ± 3.0	13.1 ± 2.8	11.1 ± 2.8	15.0 ± 3.5	14.1 ± 3.7	13.4 ± 2.3
	MFR increase (Hz)	12.9 ± 3.4	15.0 ± 3.1	12.0 ± 3.0	14.6 ± 3.5	15.6 ± 4.2	13.8 ± 4.4
	MFR decrease (Hz)	9.7 ± 2.9	11.6 ± 2.6	10.5 ± 3.0	15.1 ± 3.9	13.0 ± 3.7	12.8 ± 2.7

observed that the PC1 extracted from motor units of intrinsic muscles explained a percent of variance (of the set of spike trains of intrinsic muscles only) similar to that explained when pooling extrinsic muscles only. Accordingly, PC1 from intrinsic muscles correlated with force similarly than from extrinsic muscles (table 3). This result indicates that force can be predicted by only a subset of the investigated muscles, in agreement with the concept that a common drive underlies the activity of all involved muscles. Thus, it is possible to find all the common neural information from extrinsic muscles only, without recording intrinsic muscles, which is an important outcome for applications of myoelectric control for amputees.

The contribution of the analysed motor units in the common synaptic input, i.e. PC1, is represented in figure 5. The negative loads of motor units of FDI and ADM during tasks involving the main fingers they actuate, respectively index and little, may indicate a difference in motor control for those fingers when they are activated in a grip. However, figure 5 and these findings have a descriptive purpose only.

The little-finger pinch accounts for few of the hand motions in daily living activities (Santello *et al* 1998). Therefore, correlations between PC1 and force for the little finger-thumb pinch are functionally less relevant than for the whole-hand grasp or of the middle-index-thumb pinch. In future work, it will be relevant to compare the postural synergies found by Santello *et al* (1998) with synergies found from pools of motor neurons, also in relation to differences in functional relevance of the types of grasps.

With respect to an analysis based on amplitude of the EMG, rather than motor units, EMG decomposition separates the neural information of the efferent activity of motor neurons from the waveforms of the action potentials (represented in figure 3). The latter are influenced by many factors other than the neural drive to the muscles. Moreover, decomposition completely removes EMG crosstalk (Muceli *et al* 2014) from the analysis, which is a major factor of error in inferring neural connectivity from EMG amplitude (Farina *et al* 2004, 2014a, 2014b, Farina and Negro 2015).

The number of extracted motor units largely changed for different tasks (table 2), while MFR was less variable across tasks. The task involving the little finger presented for all muscles, except for the ADM, the lowest number of identified motor units. The number of motor units identified with HD-sEMG decomposition is only a relatively small percentage of the total number of active motor units. For example, anatomical studies indicate that the FDI has approximately 120 motor units (Enoka 1995) and the ADM more than 300 motor units (Santo Neto *et al* 1985). Moreover, the number of channels

over each muscle was different. For instance, 64 electrodes recorded the ADM while the same number of channels was used to record from three interossei muscles. Nonetheless, despite the absolute number of identified motor units does not represent the actual recruitment, the relative number of motor units extracted in each task was consistent with the performed function. For example, the greatest number of motor units for the ADM was found for tasks involving the little finger (five-digits, index-little task, little only). The number of motor units for the FDI was greater for the tasks involving the index finger and the tasks with the higher number of motor units for the interossei were those involving the index and the middle finger. In general, we could identify a smaller number of units for the extrinsic with respect to the intrinsic muscles, which is likely due to the different properties of the volume conductor at the forearm and in the hand. The different properties of the volume conductor for the muscles investigated are indeed evident when inspecting the action potential waveforms extracted by STA (figure 3). These have largely different durations, which is mostly associated to the low-pass filtering effect of the tissues interposed between the muscle fibres and the electrodes (Farina *et al* 2004). table 2 shows a higher average value of mean firing-rate discharge, during pushing on the load cell (force increasing) instead of during releasing the grip, which agrees with a vast literature of motor unit data showing smaller discharge rates at derecruitment than at recruitment (Heckman and Enoka 2012).

The STA to extract single unit action potentials across the grids provided the approximate localization of the motor units over the skin plane under the electrode grids (figure 3). In this way, it was possible, for example, to identify the three muscles composing the thenar group by the localization of their motor units.

The combination of specific directives for mounting the electrode grids and processing of the EMG signals to enable the study of neural control of the hand, in ways different than in the past, constitute the framework we present in this paper. Although it comprises technologies that have been previous described, their combination enables simultaneous observations of motor units from hand muscles, both extrinsic and intrinsic, in a way that has never been attempted before. With this work, we recommend and encourage to consider EMG decomposition of multiple muscles to observe common behaviour among a vast pool of motor neurons innervating muscles actuating several degrees of freedom, such as in the hand. Moreover, in rehabilitation technologies, such as for stroke therapy, this framework can be translated into a neural interface to provide control signals for hand exoskeletons or virtual reality. It can also be used to extract biomarkers of recovery or for monitoring the effect of therapy. The control signal provided by PC1 and the associated weights of motor neurons in PC1 may be used for functional electrical stimulation (FES) in stroke rehabilitation.

5. Conclusions

We propose the presented framework for applications in non-invasive neurophysiological studies on neural control of hand muscles in healthy and pathological conditions as well as for man-machine interfacing purposes. For example, the identified common drive to motor neurons may be used for controlling hand exoskeletons or FES devices for stroke rehabilitation. The proposed framework can easily be adapted to a wearable version with ease of application.

Funding

This work was partly supported by the European Research Council Synergy project 'Natural BionicS' (#810346). Silvia Muceli was financed by the Chalmers Life Science Engineering Area of Advance.

ORCID iDs

Silvia Muceli
https://orcid.org/0000-0002-0310-1021
Dario Farina
https://orcid.org/0000-0002-7883-2697

References

Ajiboye A B and Weir R F 2009 Muscle synergies as a predictive framework for the EMG patterns of new hand postures *J. Neural. Eng.* **6** 036004

Bergmeister K D *et al* 2017 Broadband prosthetic interfaces: combining nerve transfers and implantable multichannel EMG technology to decode spinal motor neuron activity *Frontiers Neurosci.* **11** 421

Brunton S L and Kutz J N 2019 *Data-driven Science and Engineering: Machine Learning, Dynamical Systems, and Control* (Cambridge: Cambridge University Press)

Celadon N, Dosen S, Paleari M, Farina D and Ariano P 2015 Individual finger classification from surface EMG: influence of electrode set *2015 37th Ann. Int. Conf. of the IEEE Eng. Med. Biol. Soc. (EMBC)* pp 7284–7

Celadon N, Došen S, Binder I, Ariano P and Farina D 2016 Proportional estimation of finger movements from high-density surface electromyography *J. Neuroeng. Rehabil.* **13** 73

De Luca C J 1985 Control properties of motor units *J. Exp. Biol.* **115** 125–36

De Luca C J and Erim Z 1994 Common drive of motor units in regulation of muscle force *Trends Neurosci.* **17** 299–305

Del Vecchio A, Germer C M, Elias L A, Fu Q, Fine J, Santello M and Farina D 2019 The human central nervous system transmits common synaptic inputs to distinct motor neuron pools during non-synergistic digit actions *J. Physiol.* **597** 5935–48

Del Vecchio A, Ubeda A, Sartori M, Azorin J M, Felici F and Farina D 2018 Central nervous system modulates the neuromechanical delay in a broad range for the control of muscle force *J. Appl. Physiol.* **125** 1404–10

Della Santina C, Bianchi M, Averta G, Ciotti S, Arapi V, Fani S, Battaglia E, Catalano M G, Santello M and Bicchi A 2017 Postural hand synergies during environmental constraint exploitation *Frontiers Neurorob.* **11** 41

Enoka R M and Fuglevand A J 2001 Motor unit physiology: some unresolved issues *Muscle Nerve* **24** 4–17

Enoka R M 1995 Morphological features and activation patterns of motor units *J. Clin. Neurophysiol.* **12** 538–59

Erimaki S, Agapaki O M and Christakos C N 2013 Neuromuscular mechanisms and neural strategies in the control of time-varying muscle contractions *J. Neurophysiol.* **110** 1404–14

Farina D, Arendt-Nielsen L, Merletti R and Graven-Nielsen T 2002 Assessment of single motor unit conduction velocity during sustained contractions of the tibialis anterior muscle with advanced spike triggered averaging *J. Neurosci. Methods* **115** 1–12

Farina D, Holobar A, Merletti R and Enoka R M 2010 Decoding the neural drive to muscles from the surface electromyogram *Clin. Neurophysiol.* **121** 1616–23

Farina D, Merletti R and Enoka R M 2004 The extraction of neural strategies from the surface EMG *J. Appl. Physiol.* **96** 1486–95

Farina D, Merletti R and Enoka R M 2014a The extraction of neural strategies from the surface EMG: an update *J. Appl. Physiol.* **117** 1215–30

Farina D and Negro F 2015 Common synaptic input to motor neurons, motor unit synchronization, and force control *Exercise Sport Sci. Rev.* **43** 23–33

Farina D, Negro F and Dideriksen J L 2014b The effective neural drive to muscles is the common synaptic input to motor neurons *J. Physiol.* **592** 3427–41

Farina D, Vujaklija I, Sartori M, Kapelner T, Negro F, Jiang N, Bergmeister K, Andalib A, Principe J and Aszmann O C 2017 Man/machine interface based on the discharge timings of spinal motor neurons after targeted muscle reinnervation *Nat. Biomed. Eng.* **1** 0025

Heckman C J and Enoka R M 2012 Motor unit *Compr. Physiol.* **2** 2629–82

Holobar A, Minetto M A and Farina D 2014 Accurate identification of motor unit discharge patterns from high-density surface EMG and validation with a novel signal-based performance metric *J. Neural. Eng.* **11** 016008

Holobar A and Zazula D 2007 Gradient convolution kernel compensation applied to surface electromyograms *Int. Conf. on Independent Component Analysis and Signal Separation* (Berlin: Springer) pp 617–24

Huesler E J, Maier M A and Hepp-Reymond M C 2000 EMG activation patterns during force production in precision grip. III. Synchronisation of single motor units *Exp. Brain Res.* **134** 441–55

Iberall T 1987 The nature of human prehension: three dextrous hands in one *Proc. 1987 IEEE Int. Conf. on Robotics and Automation* 4 396–401

Jolliffe I T and Cadima J 2016 Principal component analysis: a review and recent developments *Phil. Trans. R. Soc.* A **374** 20150202

Kapelner T, Negro F, Aszmann O C and Farina D 2017 Decoding motor unit activity from forearm muscles: perspectives for myoelectric control *IEEE Trans. Neural Syst. Rehabil. Eng.* **26** 244–51

Kwakkel G, Kollen B J and Krebs H I 2008 Effects of robot-assisted therapy on upper limb recovery after stroke: a systematic review *Neurorehabil. Neural Repair* **22** 111–21

Landsmeer J M F 1962 Power grip and precision handling *Ann. Rheumatic Dis.* **21** 164

Merletti R, Aventaggiato M, Botter A, Holobar A, Marateb H and Vieira T M 2010 Advances in surface EMG: recent progress in detection and processing techniques *Crit. Rev. Biomed. Eng.* **38** 4

Merletti R and Muceli S 2019 Tutorial. Surface EMG detection in space and time: Best practices *J. Electromyography Kinesiol.* **49** 102363

Meyer S, Karttunen A H, Thijs V, Feys H and Verheyden G 2014 How do somatosensory deficits in the arm and hand relate to upper limb impairment, activity, and participation problems after stroke? A systematic review *Phys. Ther.* **94** 1220–31

Muceli S, Jiang N and Farina D 2014 Extracting signals robust to electrode number and shift for online simultaneous and proportional myoelectric control by factorization algorithms *IEEE Trans. Neural Syst. Rehabil. Eng.* **22** 623–33

Napier J R 1956 The prehensile movements of the human hand *J. Bone Joint Surg. Br.* **38** 902–13

Negro F, Holobar A and Farina D 2009 Fluctuations in isometric muscle force can be described by one linear projection of low-frequency components of motor unit discharge rates *J. Physiol.* **587** 5925–38

Nordstrom M A, Fuglevand A J and Enoka R M 1992 Estimating the strength of common input to human motoneurons from the cross-correlogram *J. Physiol.* **453** 547–74

Santello M, Baud-Bovy G and Jörntell H 2013 Neural bases of hand synergies *Frontiers Comput. Neurosci.* **7** 23

Santello M, Flanders M and Soechting J F 1998 Postural hand synergies for tool use *J. Neurosci.* **18** 10105–15

Santo Neto H, De Carvalho V C and Penteado C V 1985 Motor units of the human abductor digiti minimi *Ital. J. Anat. Embryol.* **90** 47

Stegeman D F, Kleine B U, Lapatki B G and Van Dijk J P 2012 High-density surface EMG: techniques and applications at a motor unit level *Biocybern. Biomed. Eng.* **32** 3–27

Valero-Cuevas F J and Santello M 2017 On neuromechanical approaches for the study of biological and robotic grasp and manipulation *J. Neuroeng. Rehabil.* **14** 101

Weiss E J and Flanders M 2004 Muscular and postural synergies of the human hand *J. Neurophysiol.* **92** 523–35